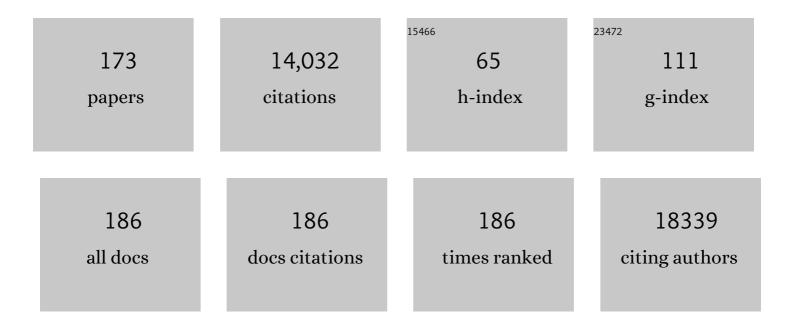
List of Publications by Year in descending order

Source: https://exaly.com/author-pdf/8002993/publications.pdf Version: 2024-02-01



#	Article	IF	CITATIONS
1	SARS-Coronavirus Replication Is Supported by a Reticulovesicular Network of Modified Endoplasmic Reticulum. PLoS Biology, 2008, 6, e226.	2.6	862
2	Complement Is Activated by IgG Hexamers Assembled at the Cell Surface. Science, 2014, 343, 1260-1263.	6.0	602
3	Nucleosomes, linker DNA, and linker histone form a unique structural motif that directs the higher-order folding and compaction of chromatin. Proceedings of the National Academy of Sciences of the United States of America, 1998, 95, 14173-14178.	3.3	500
4	Perspectives of Molecular and Cellular Electron Tomography. Journal of Structural Biology, 1997, 120, 276-308.	1.3	393
5	A molecular pore spans the double membrane of the coronavirus replication organelle. Science, 2020, 369, 1395-1398.	6.0	372
6	A unifying structural and functional model of the coronavirus replication organelle: Tracking down RNA synthesis. PLoS Biology, 2020, 18, e3000715.	2.6	368
7	Human-iPSC-Derived Cardiac Stromal Cells Enhance Maturation in 3D Cardiac Microtissues and Reveal Non-cardiomyocyte Contributions to Heart Disease. Cell Stem Cell, 2020, 26, 862-879.e11.	5.2	337
8	Renal Subcapsular Transplantation of PSC-Derived Kidney Organoids Induces Neo-vasculogenesis and Significant Glomerular and Tubular Maturation InÂVivo. Stem Cell Reports, 2018, 10, 751-765.	2.3	304
9	Three-Dimensional Transmission Electron Microscopic Observations of Mesopores in Dealuminated Zeolite Y. Angewandte Chemie - International Edition, 2001, 40, 1102-1104.	7.2	284
10	Secretory traffic triggers the formation of tubular continuities across Golgi sub-compartments. Nature Cell Biology, 2004, 6, 1071-1081.	4.6	283
11	Cryo-electron tomography of mouse hepatitis virus: Insights into the structure of the coronavirion. Proceedings of the National Academy of Sciences of the United States of America, 2009, 106, 582-587.	3.3	243
12	ER-to-Golgi Carriers Arise through Direct En Bloc Protrusion and Multistage Maturation of Specialized ER Exit Domains. Developmental Cell, 2003, 5, 583-594.	3.1	225
13	Corneal collagen fibril structure in three dimensions: Structural insights into fibril assembly, mechanical properties, and tissue organization. Proceedings of the National Academy of Sciences of the United States of America, 2001, 98, 7307-7312.	3.3	218
14	Correlative microscopy and electron tomography of GFP through photooxidation. Nature Methods, 2005, 2, 857-862.	9.0	207
15	Towards automatic electron tomography. Ultramicroscopy, 1992, 40, 71-87.	0.8	205
16	Cryoâ€electron microscopy of extracellular vesicles in fresh plasma. Journal of Extracellular Vesicles, 2013, 2, .	5.5	198
17	Automated microscopy for electron tomography. Ultramicroscopy, 1992, 46, 207-227.	0.8	188
18	Small cargo proteins and large aggregates can traverse the Golgi by a common mechanism without leaving the lumen of cisternae. Journal of Cell Biology, 2001, 155, 1225-1238.	2.3	185

#	Article	IF	CITATIONS
19	26S Proteasome Structure Revealed by Three-dimensional Electron Microscopy. Journal of Structural Biology, 1998, 121, 19-29.	1.3	183
20	Influence of aldehyde fixation on the morphology of endosomes and lysosomes: quantitative analysis and electron tomography. Journal of Microscopy, 2003, 212, 81-90.	0.8	183
21	Expression and Cleavage of Middle East Respiratory Syndrome Coronavirus nsp3-4 Polyprotein Induce the Formation of Double-Membrane Vesicles That Mimic Those Associated with Coronaviral RNA Replication. MBio, 2017, 8, .	1.8	176
22	Immuno-electron tomography of ER exit sites reveals the existence of free COPII-coated transport carriers. Nature Cell Biology, 2006, 8, 377-383.	4.6	173
23	Involvement of the Endoplasmic Reticulum in Peroxisome Formation. Molecular Biology of the Cell, 2003, 14, 2900-2907.	0.9	168
24	Integrated fluorescence and transmission electron microscopy. Journal of Structural Biology, 2008, 164, 183-189.	1.3	158
25	Influenza virus damages the alveolar barrier by disrupting epithelial cell tight junctions. European Respiratory Journal, 2016, 47, 954-966.	3.1	158
26	The Supramolecular Organization of Fibrillin-Rich Microfibrils. Journal of Cell Biology, 2001, 152, 1045-1056.	2.3	146
27	Loss of β-Cell Identity Occurs in Type 2 Diabetes and Is Associated With Islet Amyloid Deposits. Diabetes, 2015, 64, 2928-2938.	0.3	141
28	The Transformation of Enterovirus Replication Structures: a Three-Dimensional Study of Single- and Double-Membrane Compartments. MBio, 2011, 2, .	1.8	138
29	Endosomal compartmentalization in three dimensions: Implications for membrane fusion. Proceedings of the National Academy of Sciences of the United States of America, 2003, 100, 13332-13337.	3.3	136
30	The Translocon Protein Sec61 Mediates Antigen Transport from Endosomes in the Cytosol for Cross-Presentation to CD8+ T Cells. Immunity, 2015, 42, 850-863.	6.6	136
31	Heterogeneous MAC Initiator and Pore Structures in a Lipid Bilayer by Phase-Plate Cryo-electron Tomography. Cell Reports, 2016, 15, 1-8.	2.9	129
32	Structures of C1-IgG1 provide insights into how danger pattern recognition activates complement. Science, 2018, 359, 794-797.	6.0	127
33	Tools for correlative cryo-fluorescence microscopy and cryo-electron tomography applied to whole mitochondria in human endothelial cells. European Journal of Cell Biology, 2009, 88, 669-684.	1.6	125
34	Ultrastructural Characterization of Arterivirus Replication Structures: Reshaping the Endoplasmic Reticulum To Accommodate Viral RNA Synthesis. Journal of Virology, 2012, 86, 2474-2487.	1.5	121
35	Asymmetric cryo-EM reconstruction of phage MS2 reveals genome structure in situ. Nature Communications, 2016, 7, 12524.	5.8	114
36	Insights into IgM-mediated complement activation based on in situ structures of IgM-C1-C4b. Proceedings of the National Academy of Sciences of the United States of America, 2019, 116, 11900-11905.	3.3	112

#	Article	IF	CITATIONS
37	Virtual nanoscopy: Generation of ultra-large high resolution electron microscopy maps. Journal of Cell Biology, 2012, 198, 457-469.	2.3	110
38	Intradermal vaccination with hollow microneedles: A comparative study of various protein antigen and adjuvant encapsulated nanoparticles. Journal of Controlled Release, 2017, 266, 109-118.	4.8	110
39	Structural Features of 26S and 20S Proteasomes. Enzyme & Protein, 1993, 47, 252-273.	1.6	107
40	Cryoelectron Tomography of the NAIP5/NLRC4 Inflammasome: Implications for NLR Activation. Structure, 2015, 23, 2349-2357.	1.6	104
41	Quantification of nanosized extracellular membrane vesicles with scanning ion occlusion sensing. Nanomedicine, 2013, 8, 1443-1458.	1.7	102
42	Atrasentan Reduces Albuminuria by Restoring the Glomerular Endothelial Glycocalyx Barrier in Diabetic Nephropathy. Diabetes, 2016, 65, 2429-2439.	0.3	101
43	CsuA/BABCDE-dependent pili are not involved in the adherence of Acinetobacter baumannii ATCC19606T to human airway epithelial cells and their inflammatory response. Research in Microbiology, 2009, 160, 213-218.	1.0	99
44	Contribution of high-resolution correlative imaging techniques in the study of the liver sieve in three-dimensions. Microscopy Research and Technique, 2007, 70, 230-242.	1.2	97
45	Electron Tomography of Single Ice-Embedded Macromolecules: Three-Dimensional Alignment and Classification. Journal of Structural Biology, 1997, 120, 387-395.	1.3	96
46	Correlative cryo super-resolution light and electron microscopy on mammalian cells using fluorescent proteins. Scientific Reports, 2019, 9, 1369.	1.6	95
47	Postmortem MRI and histology demonstrate differential iron accumulation and cortical myelin organization in early- and late-onset Alzheimer's disease. Neurobiology of Aging, 2018, 62, 231-242.	1.5	93
48	Do Biofilm Formation and Interactions with Human Cells Explain the Clinical Success of Acinetobacter baumannii?. PLoS ONE, 2010, 5, e10732.	1.1	92
49	Golgi Enzymes Are Enriched in Perforated Zones of Golgi Cisternae but Are Depleted in COPI Vesicles. Molecular Biology of the Cell, 2004, 15, 4710-4724.	0.9	90
50	Image formation modeling in cryo-electron microscopy. Journal of Structural Biology, 2013, 183, 19-32.	1.3	90
51	Radiation damage in single-particle cryo-electron microscopy: effects of dose and dose rate. Journal of Synchrotron Radiation, 2011, 18, 398-412.	1.0	88
52	An autofocus method for a TEM. Ultramicroscopy, 1987, 21, 209-222.	0.8	85
53	Automated high-throughput electron tomography by pre-calibration of image shifts. Journal of Microscopy, 2002, 205, 187-200.	0.8	84
54	Practical autoalignment of transmission electron microscopes. Ultramicroscopy, 1992, 40, 89-107.	0.8	81

#	Article	IF	CITATIONS
55	Cryo-electron tomography in biology and medicine. Annals of Anatomy, 2009, 191, 427-445.	1.0	81
56	The nuclear lamina promotes telomere aggregation and centromere peripheral localization during senescence of human mesenchymal stem cells. Journal of Cell Science, 2008, 121, 4018-4028.	1.2	80
57	Advances in cryo-electron tomography for biology and medicine. Annals of Anatomy, 2018, 217, 82-96.	1.0	80
58	The C-terminal domain of the Pseudomonas secretin XcpQ forms oligomeric rings with pore activity. Journal of Molecular Biology, 1999, 294, 1169-1179.	2.0	77
59	Multigranular exocytosis of Weibel-Palade bodies in vascular endothelial cells. Blood, 2010, 116, 1807-1816.	0.6	76
60	Human iPSC-Derived Retinas Recapitulate the Fetal CRB1 CRB2 Complex Formation and Demonstrate that Photoreceptors and MA1⁄4ller Glia Are Targets of AAV5. Stem Cell Reports, 2019, 12, 906-919.	2.3	75
61	Tricorn Protease Exists as an Icosahedral Supermolecule In Vivo. Molecular Cell, 1997, 1, 59-65.	4.5	74
62	Electron tomography in life science. Seminars in Cell and Developmental Biology, 2009, 20, 920-930.	2.3	73
63	Correlated Light and Electron Cryo-Microscopy. Methods in Enzymology, 2010, 481, 317-341.	0.4	72
64	STEM tomography in cell biology. Journal of Structural Biology, 2007, 159, 381-391.	1.3	71
65	SP1 Protein-Based Nanostructures and Arrays. Nano Letters, 2008, 8, 473-477.	4.5	70
66	Mind the gap: Micro-expansion joints drastically decrease the bending of FIB-milled cryo-lamellae. Journal of Structural Biology, 2019, 208, 107389.	1.3	70
67	Early Stages of Golgi Vesicle and Tubule Formation Require Diacylglycerol. Molecular Biology of the Cell, 2009, 20, 780-790.	0.9	69
68	Cryo automated electron tomography: Towards highâ€resolution reconstructions of plasticâ€embedded structures. Journal of Microscopy, 1994, 174, 75-84.	0.8	68
69	Biogenesis and architecture of arterivirus replication organelles. Virus Research, 2016, 220, 70-90.	1.1	65
70	Replication of <i>Plasmodium</i> in reticulocytes can occur without hemozoin formation, resulting in chloroquine resistance. Journal of Experimental Medicine, 2015, 212, 893-903.	4.2	62
71	Three-Dimensional Electron Microscopy of Mesoporous Materials—Recent Strides Towards Spatial Imaging at the Nanometer Scale. ChemPhysChem, 2002, 3, 776-780.	1.0	61
72	Insights into complement convertase formation based on the structure of the factor B-cobra venom factor complex. EMBO Journal, 2009, 28, 2469-2478.	3.5	61

#	Article	IF	CITATIONS
73	Actin filaments are involved in the maintenance of Golgi cisternae morphology and intra-Golgi pH. Cytoskeleton, 2006, 63, 778-791. A 3D-TEM study of the shape of mesopores in SBA-15 and modified SBA-15 materialsElectronic	4.4	60
74	supplementary information (ESI) available: Fig. S1: schematic view of the MCM-41 formation mechanism. Movie S2: Aligned TEM tilt series of the SBA-15 particle from Fig. 1 (sample with the lower TEOS to) Tj ETQq0 0 C) rg <u>BT</u> /Ove	erlggk 10 Tf 5
75	Communications, 2002, , 1632-1633. Cryo electron tomography of vitrified fibroblasts: Microtubule plus ends in situ. Journal of Structural Biology, 2008, 161, 459-468.	1.3	58
76	Multidimensional View of the Bacterial Cytoskeleton. Journal of Bacteriology, 2013, 195, 1627-1636.	1.0	57
77	Pushing the resolution limits in cryo electron tomography of biological structures. Journal of Microscopy, 2012, 248, 1-5.	0.8	54
78	Autotuning of a TEM using minimum electron dose. Ultramicroscopy, 1989, 27, 251-272.	0.8	52
79	Three-dimensional localization of ultrasmall immuno-gold labels by HAADF-STEM tomography. Journal of Structural Biology, 2002, 138, 58-62.	1.3	52
80	Integrity of the Early Secretory Pathway Promotes, but Is Not Required for, Severe Acute Respiratory Syndrome Coronavirus RNA Synthesis and Virus-Induced Remodeling of Endoplasmic Reticulum Membranes. Journal of Virology, 2010, 84, 833-846.	1.5	51
81	Origins of Enterovirus Replication Organelles Established by Whole-Cell Electron Microscopy. MBio, 2019, 10, .	1.8	51
82	High-Resolution Electron Tomography Study of an Industrial Niâ^'Mo/γ-Al2O3Hydrotreating Catalyst. Journal of Physical Chemistry B, 2006, 110, 10209-10212.	1.2	49
83	Cross-membranes orchestrate compartmentalization and morphogenesis in Streptomyces. Nature Communications, 2016, 7, ncomms11836.	5.8	49
84	A 3D cellular context for the macromolecular world. Nature Structural and Molecular Biology, 2014, 21, 841-845.	3.6	47
85	Three-dimensional image reconstruction of large nuclear RNP (InRNP) particles by automated electron tomography 1 1Edited by A. Klug. Journal of Molecular Biology, 1997, 267, 570-583.	2.0	46
86	Destruction of Tissue, Cells and Organelles in Type 1 Diabetic Rats Presented at Macromolecular Resolution. Scientific Reports, 2013, 3, 1804.	1.6	46
87	Electron microscopy in cell biology: integrating structure and function. Nature Reviews Molecular Cell Biology, 2003, Suppl, SS6-10.	16.1	44
88	Template matching as a tool for annotation of tomograms of stained biological structures. Journal of Structural Biology, 2007, 158, 327-335.	1.3	41
89	Escaping Host Factor PI4KB Inhibition: Enterovirus Genomic RNA Replication in the Absence of Replication Organelles. Cell Reports, 2017, 21, 587-599.	2.9	41

90Lossâ€ofâ€function analyses defines vital and redundant functions of the <i><scp>P</scp>lasmodium</i>1.24090nomboid protease family. Molecular Microbiology, 2013, 88, 318-338.1.240

#	Article	IF	CITATIONS
91	Detection of bioorthogonal groups by correlative light and electron microscopy allows imaging of degraded bacteria in phagocytes. Chemical Science, 2016, 7, 752-758.	3.7	40
92	Human CD8 ⁺ T Cells Damage Noninfected Epithelial Cells during Influenza Virus Infection <i>In Vitro</i> . American Journal of Respiratory Cell and Molecular Biology, 2017, 57, 536-546.	1.4	40
93	Intracellular Storage and Regulated Secretion of Von Willebrand Factor in Quantitative Von Willebrand Disease. Journal of Biological Chemistry, 2011, 286, 24180-24188.	1.6	39
94	Cryo-electron tomography analysis of membrane vesicles from Acinetobacter baumannii ATCC19606T. Research in Microbiology, 2013, 164, 397-405.	1.0	39
95	Cartilage ultrastructure in proteoglycanâ€deficient zebrafish mutants brings to light new candidate genes for human skeletal disorders. Journal of Pathology, 2011, 223, 531-542.	2.1	38
96	Weibel-Palade Body Localized Syntaxin-3 Modulates Von Willebrand Factor Secretion From Endothelial Cells. Arteriosclerosis, Thrombosis, and Vascular Biology, 2018, 38, 1549-1561.	1.1	35
97	Multiple capsid-stabilizing interactions revealed in a high-resolution structure of an emerging picornavirus causing neonatal sepsis. Nature Communications, 2016, 7, 11387.	5.8	34
98	Ruthenium Polypyridyl Complexes Hopping at Anionic Lipid Bilayers through a Supramolecular Bond Sensitive to Visible Light. Chemistry - A European Journal, 2012, 18, 10271-10280.	1.7	33
99	Vitrification of Tokuyasu-style immuno-labelled sections for correlative cryo light microscopy and cryo electron tomography. Journal of Structural Biology, 2014, 186, 273-282.	1.3	32
100	AreTomo: An integrated software package for automated marker-free, motion-corrected cryo-electron tomographic alignment and reconstruction. Journal of Structural Biology: X, 2022, 6, 100068.	0.7	32
101	Automated Electron Tomography of the Septal Pore Cap in Rhizoctonia solani. Journal of Structural Biology, 2000, 131, 10-18.	1.3	31
102	A toolkit for the characterization of CCD cameras for transmission electron microscopy. Acta Crystallographica Section D: Biological Crystallography, 2010, 66, 97-109.	2.5	31
103	Correlative Cryo-Fluorescence Light Microscopy and Cryo-Electron Tomography of Streptomyces. Methods in Cell Biology, 2014, 124, 217-239.	0.5	31
104	Subcompartmentalization by cross-membranes during early growth of Streptomyces hyphae. Nature Communications, 2016, 7, 12467.	5.8	31
105	Enhanced luminescence of Ag nanoclusters via surface modification. Nanotechnology, 2013, 24, 075703.	1.3	30
106	A new approach to improve the quality of ultrathin cryo-sections; its use for immunogold EM and correlative electron cryo-tomography. Journal of Structural Biology, 2011, 175, 62-72.	1.3	29
107	Loss of CRB2 in Müller glial cells modifies a CRB1-associated retinitis pigmentosa phenotype into a Leber congenital amaurosis phenotype. Human Molecular Genetics, 2019, 28, 105-123.	1.4	29
108	3-D Structure of Multilaminar Lysosomes in Antigen Presenting Cells Reveals Trapping of MHC II on the Internal Membranes. Traffic, 2004, 5, 936-945.	1.3	28

#	Article	IF	CITATIONS
109	Microtubule Plus-End Conformations and Dynamics in the Periphery of Interphase Mouse Fibroblasts. Molecular Biology of the Cell, 2008, 19, 3138-3146.	0.9	28
110	von Willebrand factor remodeling during exocytosis from vascular endothelial cells. Journal of Thrombosis and Haemostasis, 2013, 11, 2009-2019.	1.9	28
111	Maternally supplied S-acyl-transferase is required for crystalloid organelle formation and transmission of the malaria parasite. Proceedings of the National Academy of Sciences of the United States of America, 2016, 113, 7183-7188.	3.3	28
112	Structural features of archaebacterial and eukaryotic proteasomes. Molecular Biology Reports, 1995, 21, 11-20.	1.0	26
113	Imaging complement by phase-plate cryo-electron tomography from initiation to pore formation. Journal of Structural Biology, 2017, 197, 155-162.	1.3	26
114	Optimisations and Challenges Involved in the Creation of Various Bioluminescent and Fluorescent Influenza A Virus Strains for In Vitro and In Vivo Applications. PLoS ONE, 2015, 10, e0133888.	1.1	26
115	Three-dimensional Architecture of Hair-bundle Linkages Revealed by Electron-microscopic Tomography. JARO - Journal of the Association for Research in Otolaryngology, 2008, 9, 215-224.	0.9	24
116	Conical Fourier shell correlation applied to electron tomograms. Journal of Structural Biology, 2015, 190, 215-223.	1.3	24
117	Graphene Liquid Cells Assembled through Loopâ€Assisted Transfer Method and Located with Correlated Lightâ€Electron Microscopy. Advanced Functional Materials, 2020, 30, 1904468.	7.8	24
118	Novel localization of Rab3D in rat intestinal goblet cells and Brunner's gland acinar cells suggests a role in early Golgi trafficking. American Journal of Physiology - Renal Physiology, 2007, 293, G165-G177.	1.6	23
119	Capsids of Tricorn Protease Studied by Electron Cryomicroscopy. Journal of Structural Biology, 1999, 128, 65-68.	1.3	22
120	Ultrastructural Imaging of <i>Salmonella</i> –Host Interactions Using Superâ€resolution Correlative Lightâ€Electron Microscopy of Bioorthogonal Pathogens. ChemBioChem, 2018, 19, 1766-1770.	1.3	19
121	Overview of computer-aided electron microscopy. Ultramicroscopy, 1992, 46, 189-197.	0.8	18
122	Predicted secondary structure of the 20 S proteasome and model structure of the putative peptide channel. FEBS Letters, 1994, 354, 45-49.	1.3	18
123	A vaccinia virus lacking A10L: viral core proteins accumulate on structures derived from the endoplasmic reticulum. Cellular Microbiology, 2006, 8, 427-437.	1.1	17
124	Fluorescent labeling of resin-embedded sections for correlative electron microscopy using tomography-based contrast enhancement. Journal of Structural Biology, 2008, 161, 372-383.	1.3	17
125	Content delivery to newly forming Weibel-Palade bodies is facilitated by multiple connections with the Golgi apparatus. Blood, 2015, 125, 3509-3516.	0.6	17
126	CRB2 Loss in Rod Photoreceptors Is Associated with Progressive Loss of Retinal Contrast Sensitivity. International Journal of Molecular Sciences, 2019, 20, 4069.	1.8	16

#	Article	IF	CITATIONS
127	Progression and Classification of Granular Osmiophilic Material (GOM) Deposits in Functionally Characterized Human NOTCH3 Transgenic Mice. Translational Stroke Research, 2020, 11, 517-527.	2.3	16
128	Cryotomography: Low-dose Automated Tomography of Frozen-hydrated Specimens. , 2007, , 113-161.		16
129	MAVIS: An integrated system for live microscopy and vitrification. Ultramicroscopy, 2014, 143, 67-76.	0.8	15
130	Mammalian orthoreovirus T3D infects U-118 MG cell spheroids independent of junction adhesion molecule-A. Gene Therapy, 2014, 21, 609-617.	2.3	15
131	Localization of active endogenous and exogenous βâ€glucocerebrosidase by correlative lightâ€electron microscopy in human fibroblasts. Traffic, 2019, 20, 346-356.	1.3	15
132	Bioorthogonal Correlative Light-Electron Microscopy of <i>Mycobacterium tuberculosis</i> in Macrophages Reveals the Effect of Antituberculosis Drugs on Subcellular Bacterial Distribution. ACS Central Science, 2020, 6, 1997-2007.	5.3	15
133	Correction of autofocusing errors due to specimen tilt for automated electron tomography. Journal of Microscopy, 2003, 211, 179-185. Three-Dimensional Transmission Electron Microscopic Observations of Mesopores in Dealuminated	0.8	14
134	Zeolite Y Supported by NWO under grant 98037. The research of A.J.K. has been made possible by a fellowship of the Royal Netherlands Academy of Arts and Sciences (KNAW). The authors thank J. E. M. J. Raaymakers for the nitrogen physisorption measurements, A. J. M. Mens for the XPS measurements, J. A. R. van Veen and E. J. Crevghton for physical data and useful discussions, and Shell International	7.2	14
135	Chemicals and Zeol. Angewandte Chemie - International Edition, 2001, 40, 1102-1104. Automated vitrification of cryo-EM samples with controllable sample thickness using suction and real-time optical inspection. Nature Communications, 2022, 13, .	5.8	14
136	Correlative light and electron microscopy reveals discrepancy between gold and fluorescence labelling. Journal of Microscopy, 2017, 267, 309-317.	0.8	13
137	Automated Electron Tomography of Large Nuclear RNP (InRNP) Particles—The Naturally Assembled Complexes of Precursor Messenger RNA and Splicing Factors. Journal of Structural Biology, 1997, 120, 228-236.	1.3	12
138	Inducing fluorescence of uranyl acetate as a dual-purpose contrast agent for correlative light-electron microscopy with nanometre precision. Scientific Reports, 2017, 7, 10442.	1.6	11
139	Correlative microscopy for structural microbiology. Current Opinion in Microbiology, 2018, 43, 132-138.	2.3	11
140	Electron tomographic reconstruction of plastic-embedded organelles involved in the chitin secretion process. Biology of the Cell, 1996, 88, 5-13.	0.7	10
141	Glomerular permeability is not affected by heparan sulfate glycosaminoglycan deficiency in zebrafish embryos. American Journal of Physiology - Renal Physiology, 2019, 317, F1211-F1216.	1.3	10
142	Super-resolution correlative light-electron microscopy using a click-chemistry approach for studying intracellular trafficking. Methods in Cell Biology, 2021, 162, 303-331.	0.5	10
143	Cellular Nanoimaging by Cryo Electron Tomography. Methods in Molecular Biology, 2013, 950, 227-251.	0.4	9
144	Defining Phenotype, Tropism, and Retinal Gene Therapy Using Adeno-Associated Viral Vectors (AAVs) in New-Born Brown Norway Rats with a Spontaneous Mutation in Crb1. International Journal of Molecular Sciences, 2021, 22, 3563.	1.8	9

#	Article	IF	CITATIONS
145	EDITORIAL. Journal of Structural Biology, 1997, 120, 207-209.	1.3	8
146	Electron tomography of molecular sieves. Studies in Surface Science and Catalysis, 2005, 157, 225-242.	1.5	8
147	Towards the imaging of Weibel–Palade body biogenesis by serial block faceâ€scanning electron microscopy. Journal of Microscopy, 2015, 259, 97-104.	0.8	8
148	Distinct antigen uptake receptors route to the same storage compartments for crossâ€presentation in dendritic cells. Immunology, 2021, 164, 494-506.	2.0	8
149	Three-Dimensional Transmission Electron Microscopic Observations of Mesopores in Dealuminated Zeolite Y. Angewandte Chemie - International Edition, 2001, 40, 1102-1104.	7.2	8
150	Academic Colloquium on Electron Tomography. Journal of Structural Biology, 2002, 138, 1-5.	1.3	6
151	Defocus estimation from stroboscopic cryo-electron microscopy data. Ultramicroscopy, 2011, 111, 1592-1598.	0.8	6
152	Correlative Light Microscopy and Electron Tomography to Study Von Willebrand Factor Exocytosis from Vascular Endothelial Cells. Methods in Cell Biology, 2014, 124, 71-92.	0.5	6
153	Correlated Cryo Superâ€Resolution Light and Cryoâ€Electron Microscopy on Mammalian Cells Expressing the Fluorescent Protein rsEGFP2. Small Methods, 2019, 3, 1900425.	4.6	6
154	Doublecortinâ€like expressing astrocytes of the suprachiasmatic nucleus are implicated in the biosynthesis of vasopressin and influences circadian rhythms. Glia, 2021, 69, 2752-2766.	2.5	6
155	Application of a Highly Selective Cathepsin S Two-step Activity-Based Probe in Multicolor Bio-Orthogonal Correlative Light-Electron Microscopy. Frontiers in Chemistry, 2020, 8, 628433.	1.8	5
156	The adapter protein Myd88 plays an important role in limiting mycobacterial growth in a zebrafish model for tuberculosis. Virchows Archiv Fur Pathologische Anatomie Und Physiologie Und Fur Klinische Medizin, 2021, 479, 265-275.	1.4	5
157	Editorial on Correlative microscopy. Ultramicroscopy, 2014, 143, 1-2.	0.8	4
158	The potential of bioorthogonal chemistry for correlative light and electron microscopy: a call to arms. Journal of Chemical Biology, 2015, 8, 153-157.	2.2	4
159	Preliminary Three-Dimensional Model of Insect Lipoprotein HDLp by Using Electron Microscopy and X-ray Crystallography. Microscopy and Microanalysis, 2004, 10, 1514-1515.	0.2	3
160	Singleâ€Walled Carbon Nanotubes as Scaffolds to Concentrate DNA for the Study of DNA–Protein Interactions. ChemPhysChem, 2012, 13, 1569-1575.	1.0	3
161	Recent advances in electron tomography. Journal of Structural Biology, 2017, 197, 71-72.	1.3	3
162	Nanofabrication of a gold fiducial array on specimen support for electron tomography. Ultramicroscopy, 2013, 135, 99-104.	0.8	2

#	Article	IF	CITATIONS
163	ENZEL - A cryogenic, retrofittable, coincident fluorescence, electron, and ion beam solution for the cryo-electron tomography workflow Microscopy and Microanalysis, 2021, 27, 3228-3229.	0.2	2
164	Orthogonal Functionalization of Ferritin via Supramolecular Reâ€Assembly. European Journal of Inorganic Chemistry, 2015, 2015, 4603-4610.	1.0	1
165	Fluorescence-guided lamella fabrication with ENZEL, an integrated cryogenic CLEM solution for the cryo-electron tomography workflow. Microscopy and Microanalysis, 2021, 27, 3234-3235.	0.2	1
166	Title is missing!. , 2020, 18, e3000715.		1
167	Quantitative Analysis of the Influence of Aldehyde Pre-Fixation on the Morphology of Endosomes and Lysosomes. Microscopy and Microanalysis, 2003, 9, 500-501.	0.2	0
168	Cutting the cost of high-resolution microscopy. Nature Materials, 2005, 4, 885-886.	13.3	0
169	Zooming in on Cell Architecture and Molecular Structures with Correlative Light and Electron Microscopy. Microscopy and Microanalysis, 2018, 24, 874-875.	0.2	0
170	Imaging of Von Willebrand Factor Remodeling Upon Secretion From Vascular Endothelial Cells. Blood, 2012, 120, 263-263.	0.6	0
171	Title is missing!. , 2020, 18, e3000715.		0
172	Title is missing!. , 2020, 18, e3000715.		0
173	Title is missing!. , 2020, 18, e3000715.		0